# Heterogeneous Time Dependent Static Light Scattering

**Ruth Schimanowski,† Roland Strelitzki, David A. Mullin,‡ and Wayne F. Reed***

*Physics Department, Tulane University, New Orleans, Louisiana 70118*

*Received May 18, 1999; Revised Manuscript Received August 3, 1999*

ABSTRACT: Measurements of light scattering from flowing heterogeneous solutions containing coexisting populations of colloids and polymers are presented. By appropriate recognition of scattering peaks produced by individual colloid particles and recovery of the baseline scattering due to the polymer population, the colloid particle number density can be monitored in real time while the polymer population is characterized absolutely according to weight-average molecular weight $M_w$, and $z$-average mean square radius of gyration $\langle S^2 \rangle_z$. Either or both populations may also be evolving in time, so that the technique is termed "heterogeneous time dependent static light scattering" (HTDSLS). The essential notions of the technique are presented, and then the feasibility of the simultaneous measurements is first demonstrated by an equilibrium characterization of poly(vinylpyrrolidone) (PVP) "contaminated" by known concentrations of 2 $\mu$m latex spheres. The time dependent capabilities are then demonstrated by monitoring the growth of *Escherichia coli* bacteria in a solution containing PVP. It is expected that HTDSLS will find many applications, such as in biotechnology reactors, biomedical assays, and polymer reactors where gels or crystallites are produced in addition to polymer chains.

## Introduction

Classical static light scattering (SLS) in polymer and colloid solutions has generally addressed the problem of finding equilibrium properties, specifically, average molecular masses, interaction coefficients, dimensions, and shape factors. Recently, more attention has been paid to making time-dependent static light-scattering (TDSLS) measurements on solutions undergoing such nonequilibrium processes as polymerization,[1] degradation,[2−5] aggregation,[6−8] gelation,[9] and phase separation.[10]

Nonequilibrium processes occur in a wide variety of situations in biomedical, biotechnological, pharmaceutical, food, paint, coatings, water purification, polymer, and other industries. In both SLS and TDSLS up until now, solutions must normally be *homogeneous*. That is, it is usually assumed that only one species of particle is present, even though these may contain a wide distribution of masses, sizes, etc. A notable exception is the case where one of the species is isorefractive with the solvent, so that only the other species scatters. An approach to mixed polymer/colloid systems has also been presented by theoretically manipulating the total scattering curves from such solutions, as opposed to experimentally separating each signal.[11]

In this work we marry the SLS and TDSLS technologies with those from single particle detection, to allow time-dependent scattering measurements to be made from heterogeneous systems. This technique may be termed heterogeneous time dependent static light scattering or HTDSLS. HTDSLS should allow accurate, real-time measurements on many systems of interest, which until now could not be characterized by SLS or TDSLS.

The basic notion is that there will be a homogeneous population of polymer or small colloids, together with a much less numerous population of large particles. All else being equal, particle scattering at low angles increases as the sixth power of a solid particle's radius. Hence, for example, a single solid particle of 1 $\mu$m radius could scatter as much as $10^{18}$ enzymes of radius 1 nm. This scattering from a single cell might be much larger than the scattering from all the enzymes in the scattering volume. But the cell diffuses about, whereas the enzyme background remains essentially constant as long as there are a large number of enzymes in the scattering volume. Hence when a cell diffuses into the volume there will be a large increase in scattering intensity, which will then disappear when the cell diffuses out of the volume. This increase in intensity may appear as a spike or a more irregular shape. The profile of light scattered from the cell can be guaranteed to look like a spike if there is relative motion between the sample solution and the incident light beam used in the scattering experiment. In fact, using flowing solutions containing large particles to produce spikes has already been exploited in single particle detection.

We wish to both count the spikes, as in single particle counting, and measure the absolute scattering from the homogeneous polymer background. We also wish to do this under conditions where the characteristics of both the homogeneous and large particle populations might be changing in time and possibly even where new populations are being generated.

Many applications can be envisioned: (1) Bacteria (the large particles) produce industrially important polysaccharides in a biotechnology fermentation reactor. In this case both populations change in time. (2) A bacterium or yeast cell digests the polymer and reproduces. In this case the large particle count increases and the homogeneous scattering decreases. This is typical of fermentation reactions. (3) A certain polymer causes blood cells to aggregate. Here the large particle population count decreases but individual spike sizes increase. (4) A polymer is being produced, but at the same time large impurities, such as gels or crystallites, are also being formed. Resolution of the two populations could indicate the origin of the impurities. There are many more possible scenarios.

* To whom correspondence should be addressed.
† On leave from Freie Universität Berlin.
‡ Present address: Department of Cell and Molecular Biology, Tulane University.

10.1021/ma9907690 CCC: $18.00 
Published on Web 09/23/1999

After a brief summary of relevant scattering relations, the first part of this work lays out the technical notions and requirements for HTDSLS and describes the system built to accomplish this, and the second part presents experimental results on different heterogeneous polymer/colloid solutions.

## Background Theory

The characterization of the background polymer population (BP) is made according to the procedures and theories developed over the last half century. SLS has been used for many years as a means of absolute characterization of colloids and polymers. The most useful set of approximations for polymer characterization are due to Zimm,[12] and Rayleigh and Debye.[13] In these approximations, it is assumed that the intraparticle interference for light waves scattered from a single particle and reaching a detector is due solely to the difference in geometrical path $\delta$, for the light waves; i.e.

$$\delta = \frac{2\pi a|\frac{n_p}{n_s} - 1|}{\lambda} \ll 1 \tag{1}$$

where $a$ is the characteristic dimension of the particle, $\lambda$ is the vacuum wavelength of the incident light, and $n_p$ and $n_s$ are the indices of refraction of the particle and solvent, respectively. This is a robust and widely applicable approximation for polymers, because they are generally "threadlike" entities immersed in a sea of solvent, so that the optical and geometrical path differences are virtually identical, up to a constant factor equal to $n_s$. The well-known Zimm equation,[12] which results from this approximation and the assumption of single contacts between polymers as the dominant mode of interaction at low concentrations, is

$$\frac{Kc}{I(q)} = \frac{1}{MP(q)} + 2A_2c \tag{2}$$

where $I$ is the excess Rayleigh scattering ratio (in $cm^{-1}$) and $K$ is a constant, given for vertically polarized light by

$$K = \frac{4\pi^2 n^2 (dn/dc)^2}{N_A \lambda^4} \tag{3}$$

Here $n$ is the index of refraction of the pure solvent, $\lambda$ the vacuum wavelength of the incident light, $N_A$ is Avogadro's number, and $dn/dc$ is the differential refractive index of the polymer in the pure solvent. The magnitude of the scattering vector **q**, is

$$q = \left(\frac{4\pi n}{\lambda}\right) \sin(\theta/2) \tag{4}$$

In the above theory there are no assumptions about the particle shape or mass distribution, and these enter explicitly only in the scattering form factor $P(q)$. At sufficiently low scattering angles, when the product of the particle's $z$-averaged mean square radius of gyration $\langle S^2\rangle_z$ and $q^2$ is much less than unity, then the following equation holds for *any* particle shape:

$$\frac{Kc}{I(q)} = \frac{1}{M_w}\left[1 + \frac{q^2\langle S^2\rangle_z}{3}\right] + 2A_2c \tag{5}$$

In contrast, the characterization of the large particles (LP) in its simplest form is to merely count the particles via the scattering spikes they produce, to ascertain the particle number density. Beyond this, however, the actual magnitude and angular distribution of scattered light will rest upon the details of the Mie scattering involved.[13] This theory is based on the exact solution to Maxwell's equations for the particular particle geometry and composition involved. For spherical particles, the absolute, angular dependent scattering function depends only on the ratio of $\lambda/R$, where $R$ is the particle radius, and of $n_p/n_s$ where $n_p$ and $n_s$ may be complex (i.e., involve light absorption in addition to refraction). Hence, to progress beyond particle counting for the LP requires model-dependent assumptions about the scatterers. For many scatterers, such as bacteria and yeast, the assumption of sphericity may be reasonable.

For spherical scatterers, the angular intensity in the plane perpendicular to the direction of polarization of the incident light is

$$I_s(\text{horizontal plane}) = \frac{\lambda^2}{4\pi^2 r^2}|S_1^2| \tag{6}$$

where

$$S_1 = \sum_{n=1}^{\infty} \frac{2n+1}{n(n+1)}\{a_n\pi_n(\cos\theta) + b_n\tau_n(\cos\theta)\} \tag{7}$$

and

$$\pi_n(\cos\theta) = \frac{P_n(\cos\theta)}{\sin\theta}$$
$$\tau_n(\cos\theta) = \frac{dP_n(\cos\theta)}{d\theta} \tag{8}$$

where $P_n(\cos\theta)$ are the Legendre polynomials and

$$a_n = \frac{\psi_n(\alpha)\psi_n'(\beta) - m\psi_n(\beta)\psi_n'(\alpha)}{\zeta_n(\alpha)\psi_n'(\beta) - m\psi_n(\beta)\zeta_n'(\alpha)} \tag{9a}$$

$$b_n = \frac{m\psi_n(\alpha)\psi_n'(\beta) - \psi_n(\beta)\psi_n'(\alpha)}{m\zeta_n(\alpha)\psi_n'(\beta) - \psi_n(\beta)\zeta_n'(\alpha)} \tag{9b}$$

where

$$\alpha = \frac{2\pi n_s R}{\lambda}, \quad \beta = \frac{2\pi n_p R}{\lambda}, \quad m = \frac{n_p}{n_s} \tag{10}$$

$$\psi_n(\alpha) = \sqrt{\frac{\alpha\pi}{2}} J_{n+1/2}(\alpha) \tag{11}$$

where $J_{n+1/2}$ is the Ricatti−Bessel function. The $\psi_n(\alpha)$ values obey the recursion relations[14]

$$\psi_{n+1}(x) = \frac{2n+1}{x}\psi_n(x) - \psi_{n-1}(x) \tag{12a}$$

$$\psi_n'(x) = \frac{-n}{x}\psi_n(x) + \psi_{n-1}(x) \tag{12b}$$

Finally,

$$\zeta_n(\alpha) = i^{(n+1)}e^{-i\alpha}, \quad \zeta_n'(\alpha) = i^n e^{-i\alpha} \tag{13}$$

where $i = \sqrt{-1}$.

The assumption of single scattering—that is, that a photon only scatters once before being detected—is implicit in the above theories. Hence there is a limit to the turbidity of a solution whose scattering can be analyzed by these theories. Being based on these theories, the HTDSLS technique presented in this work likewise requires that only single scattering occur.

### Summary of Particle Counting and Sizing Techniques

As early as the 1930's Moldovan[15] described a photoelectric technique to count particles flowing through a capillary. Lines[16] has more recently given a review of most particle counting and sizing methods. Many techniques employ light for investigation using blockage, and static and dynamic scattering.[17] These are useful over a broad range of sizes from 10 nm to ~1 mm. Other techniques include chromatography and those based on resistive or electrical measurements.[18,19] In the latter case, particles suspended in an electrolyte pass through a sensing aperture and produce pulses, their height being proportional to the particle volume. Gear and Bednarek[20] found that cells with diameters as low as 0.45$\mu$m can still be accurately measured. Bryant et al.[21] found a volume of 0.62 $\mu m^3$ for *Escherichia coli* cells, using the electrical method.

As discussed above, scattering from large particles requires use of the Mie theory. Therefore, particle-sizing light-scattering instruments measure scattering at angles as small as possible. For the investigation of shape and orientation, either the state of polarization of the scattered light[22] or its spatial distribution should be assessed.[23] They can be separated into different methods, which are investigations of polar scattering in a single azimuthal plane, azimuthal scattering at a single polar angle, and combinations of the two methods. LS intensity measurements in a single plane are most commonly used. For instance Gebhart et al.[24] developed a low-angle system ($\theta < 7.5°$) with a measurement volume of 0.01 $cm^3$, allowing particle concentrations of $10^4$ to be detected with a lower detection limit of 0.17 $\mu$m. An example for a completely automated device is the Hiac/Royco Optisizer, which measures particles with sizes from 0.5 to 350 $\mu$m.[25] For particles up to 1.63 $\mu$m forward scattering is used, and above this size, extinction measurements are used. The system provides a constant flow of 0.01−100 mL/min and dilution from highly concentrated solutions up to 10000:1 to avoid saturation.

Research on unicellular microorganisms by Wyatt[26] led to the development of a new device. Limited discrimination of particle shape has been shown to be possible using opposed detectors by comparing the detector output of pairs at the same angle.[27] A device allowing the measurement of LS for almost the complete 360° was described by Marshall et al.[28] There the scattered light is intercepted by an ellipsoidal mirror which directs the light through a rotating aperture (360° in 20 ms) to a photomultiplier. Measurement errors lie within 1% for particles 11 $\mu m > d > 0.3$ $\mu$m.

Wyatt et al.[29] introduced a device that has a spherical measurement chamber with 18 small apertures for detectors on each of four azimuthal planes set equidistant apart by 45°. Additionally, two large apertures at 25 and 155° are available at the same azimuthal plane. Hirst and Kaye[30] developed a system with a CCD camera, allowing 83% of the complete spatial scattering profile to be assessed.

Holve and Self,[31] who developed a low-angle scattering system, discuss in detail the whole range of difficulties associated with stray light, nonuniform laser beam, and scattering volume. They also analyze coincidence effects, which can also be a problem with the Coulter counter method.[32]

Flow cytometry allows information to be obtained on subcellular components, and multiple methods are combined to rapidly assess cells (up to $3 \times 10^5$/min).[33] Analysis techniques are usually based on electrical and optical methods, such as electronic cell volume, fluorescence from stains bound to cells, light scattering, and extinction. Additionally, cells are often separated from heterogeneous population using a cell sorting technique. Flow cytometry was used to investigate the influence of plasmids in *E. coli* cells.[34] Light-scattering measurements were used to determine the size distribution and fluorescence measurements on stained cells in order to assess their DNA content.

Since *E. coli* cells are used in this work, previous studies using light scattering are of interest. Cross and Latimer[35] measured the angular dependence of such cells between 10 and 90°, and the scattering curves were in good agreement with a modified Rayleigh−Debye approximation when the cells where modeled as coated ellipsoids. For the model the typical dimensions for the cells ($l = 2.16$ $\mu$m and $d = 0.74$ $\mu$m) were determined by microphotography and literature values for the volume. Concentration determination of bacteria includes direct counting by light microscopy, spectrophotometry, conductivity (such as with the Coulter Counter), and measurement of colony forming units per milliliter as determined by spreading diluted samples on agar plates and counting the colonies that form.

## Materials and Methods

**Polymers and Colloids Used.** Poly(vinyl pyrrolidone), or PVP, was from Sigma. A value of d*n*/d*c* of 0.173 was used. The 2 $\mu$m latex spheres from Duke Scientific Corp. were used as a stable colloid population for the spike-counting characterization of the system and for measurements of a heterogeneous colloid/polymer system in equilibrium. Their nominal concentration (supplied by the manufacturer) was $1.14 \times 10^9$ particles/$cm^3$ ± 10%.

*E. coli* strain DH5α (Bethesda Research Laboratories, Life Sciences, Inc.) was cultured in L broth which is composed of 1% Bacto tryptone, 0.5% Bacto yeast extract, 0.5% NaCl, and 0.02% $MgSO_4$.[36] Stationary phase broth cultures were prepared by inoculating cells of an *E. coli* colony into 5 mL of sterile L broth which was incubated with rotary shaking at 30 °C for 12−14 h. Stationary phase cultures were diluted into fresh L broth and used as a source of *E. coli* cells for light-scattering experiments.

**Light-Scattering Chamber.** The basic construction of the multiangle scattering chamber has been detailed in recent work.[37] In this cell optical fibers were used for detection. Detection angles were 39, 56, 73, 90, 124, and 141°. A circularized, vertically polarized 30 mW diode laser, with a vacuum wavelength of 677 nm, was used. A lens of focal length 7 cm was used to focus the beam at the center of the scattering chamber. The fluid flow in the chamber is perpendicular to the laser beam.

In cylindrical coordinates, the laser beam profile along the *z*-axis of propagation is

$$I(r,z) = \left(\frac{w_o}{w(z)}\right)^2 I_o \exp[-2r^2/w(z)^2] \quad (14)$$

where $I_o$ and $w_o$ are the beam intensity and waist, respectively, at the focal point of the beam in the center of the chamber, and $r$ is the distance from the $z$ axis. A detailed intensity map provided by the laser manufacturer allowed a value of $w_o = 40\ \mu$m to be determined.

The cylindrical scattering volume $V_s$ in this chamber is limited by the length of the scattering volume $z_m$, and is further defined by the radius $r(f)$, at which the incident beam intensity has fallen to a specified fraction $f$, of its maximum intensity

$$V_s = \pi r(f)^2 z_m \quad (15)$$

where

$$f = I(r)/I_o \quad (16)$$

For example, for $f = e^{-2}$, $r(f) = w_o$ at $z = 0$. $z_m$ is given by the diameter of the acceptance cone, which likewise defines the acceptance of $r$ in the vertical direction (which is the direction of polarization of the laser beam). This cone is defined by the optical fiber diameter $D$, the radius of the scattering chamber $R$, and the acceptance angle of the fiber $\theta_A$. At a scattering angle $\theta$, $z_m$ is given by

$$z_m = \left(R + \frac{D}{2\tan\theta_A}\right)\sin\theta\left[\frac{1}{\tan(\theta-\theta_A)} - \frac{1}{\tan(\theta+\theta_A)}\right] \quad (17)$$

where

$$\theta_A = \sin^{-1}\left(\frac{\sqrt{n_c^2 - n_{cl}^2}}{n_s}\right) \quad (18)$$

where $n_s$, $n_c$, and $n_{cl}$ are the indices of refraction of the solvent and the fiber optic core and cladding, respectively. At the usual reference angle of $\theta = 90°$, $z_m$ reduces to

$$z_m(90°) = D + 2R\tan(\theta_A) \quad (19)$$

It is also seen that for a zero acceptance angle ($\theta_A = 0$, which is equivalent to using a deep "pinhole" for detection), the scattering volume, which is proportional to $z_m$, will be proportional to 1/(sin $\theta$), which is a familiar result in scattering practice.

For this cell $z_m = 0.19$ cm. This gives a scattering volume of 9.6 nL within which the intensity is $\geq I_o e^{-2}$. In this work the actual value of $V_s$ is defined according to particle counting and/or baseline recovery criteria discussed below. The cross-sectional area perpendicular to the flow, $a(f)$, of a specified scattering volume is

$$a(f) = 2r(f)z_m \quad (20)$$

It is important to point out that the value of $q^2$ used in a Zimm plot representation is averaged over the acceptance angle of the optical fiber and weighted by the scattering power at a scattering angle $\theta$, $\langle q^2(\theta)\rangle_{power}$. It is straightforward to show that

$$\frac{\langle q^2(\theta)\rangle_{power}}{\left(\frac{4\pi n}{\lambda}\right)^2} = \frac{1}{2} - \frac{\sin(\theta+\theta_A) - \sin(\theta-\theta_A)}{4\theta_A} \cong \sin^2(\theta/2), \quad \text{to second order in } \theta_A \quad (21)$$

The difference between $q^2(\theta)$ and $\langle q^2(\theta)\rangle_{power}$ varies by less than 1% from the value of $q^2$ evaluated at $\theta$ over the scattering chamber's angular range. Hence, we are justified in simply using $q^2(\theta)$ in the Zimm plot representations which follow.

Because the current system uses a focused, circular Gaussian beam to reduce scattering volume, possible effects of the noncylindrical shape of the beam should be taken into account. The distance from the $z$ axis at which the laser intensity is a fraction $f$ of the full intensity is defined via eqs 14 and 16 as

$$r^2(z) = \frac{-w(z)^2}{2}\ln[f(1+\alpha z^2)] \quad (22a)$$

with the condition

$$f(1+\alpha z^2) \leq 1 \quad (22b)$$

where

$$w(z)^2 = w_o^2[1+\alpha z^2] \quad (23)$$

and

$$\alpha = \frac{\lambda^2}{\pi^2 w_o^4} \quad (24)$$

The cross-sectional area of the laser beam $a(f)$, over which the laser intensity is greater than or equal to $f$ and which enters in the formulas of the preceding section, is, hence

$$a(f) = 2\sqrt{2}w_o^2\int_0^{z_2}(1+\alpha z^2)^{1/2}\sqrt{-\ln[f(1+\alpha z^2)]}\,dz \quad (25a)$$

where condition 22b leads to

$$z_2 = z_m/2, \quad \text{if } \sqrt{\frac{1-f}{\alpha f}} > z_m/2 \quad (25b)$$

and

$$z_2 = \sqrt{\frac{1-f}{\alpha f}}, \quad \text{if } \sqrt{\frac{1-f}{\alpha f}} < z_m/2 \quad (25c)$$

Likewise, a volume in which the laser intensity is greater than or equal to a fraction $f$, of the full intensity is found by integrating $r^2(z)$ above over $z$, yielding

$$V_s(f) = -\pi w_o^2\left\{(z_2 + \alpha z_2^3/3)\ln[f(1+\alpha z_2^2)] - \frac{4}{3}z_2 - \frac{2}{9}\alpha z_2^3 + \frac{4}{3\sqrt{\alpha}}\tan^{-1}(\sqrt{\alpha}z)\right\} \quad (26)$$

where $z_2$ obeys conditions 25b,c.

The current apparatus, with $D = 0.1$ cm, $\lambda = 6.77 \times 10^{-5}$cm, and a lens of focal length 7 cm, gives $\alpha = 1.81$ cm$^{-2}$. Substituting into eq 23 gives an increase of the beam waist over $z_2 = 0.095$ cm of 1.6% and a volume increase, according to eq 26, of only 0.35%. Hence, we are justified in treating the beam as a cylinder over the detection volumes used.

Absence of flare light in the chamber was checked by using various solvents of known Rayleigh ratio, per the method of Florenzano et al.[1] The ability of the chamber to yield correct molecular weight values was verified by using 51 500 g/mol poly(ethylene oxide), or PEO (American Polymer Standards Co, Mentor, OH). Measurements were within 3% of this nominal value. The value of d$n$/d$c$ for the PEO was taken as 0.142 cm$^3$/g.

Data were collected using a 12-bit A/D board, for which we developed data acquisition and storage software. Typically, sampling at 20 Hz was adequate for resolving peaks, for flow rates around 0.010 cm$^3$/s. Rates of 250 Hz were used to assess peak widths. Storing in random access files at 20 Hz generated roughly 1 MB of data per hour.

The experiments were performed in a circulating setup where the solutions were pumped perpendicular to the laser beam and against gravity with a peristaltic pump (Masterflex C/L pump, model 77120-60) using typical flow rates of 10−13 $\mu$L/s. For the Zimm Plots, four to five different low concentrations of PVP were prepared from a stock solution obtained by dissolving dry PVP in aqueous solution of 0.1 M $NH_4NO_3$ and 0.5% $NaN_3$. Millex-GS 0.22 $\mu$m and Millex-VV 0.1 $\mu$m pore size sterile filters were used to prefilter the polymer solutions into dust-free vials. Dilutions of large particles were then carefully added. No online filters can be used in the recirculation apparatus, so that the colloids are not blocked. Similarly the broth that is kept at 38 °C in a water bath is prefiltered before diluted *E.coli* cells are added. Dilutions of *E. coli* cells were made from *E. coli* saturated stock solutions. The cells were diluted to about $10^{-5}$ of their concentration in the saturated solutions for the light-scattering measurements.

**Requirements and Considerations for Simultaneous Characterization of Large Particles and Background Population.** The chief requirements for making HTDSLS feasible are as follows: (1) The scattering volume must be such that the average number of large particles (LP) in the scattering volume per sampling period is less than one. For very sparse LP populations the scattering volume may be quite large, whereas for a high density of LP, the scattering volume must be small. The diffraction limit of focusing Gaussian laser beams will define the lowest practical scattering volume. (2) To form spikes from the LP, it is necessary for there to be relative motion between the LP and the beam. The relative motion is most easily provided by flowing the sample through a flow cell with a fixed laser beam and fixed photodetector(s).

The requirement that there be a significant amount of time during which there are no particles in the scattering volume can be treated as follows: We term the time during which there are no LP in the scattering volume the "clear window time" (CWT). CWT is also necessary to recover the baseline scattering from the homogeneous population of scatterers. The binomial distribution allows the fraction of time for which there are $k$ particles in the scattering detection volume, $V_s$, where $m = V_s/V_p$, to be computed for a given number concentration, $n$, of randomly distributed LP, each of volume $V_p$:

$$P(k,m,n) = (nV_p)^k (1 - nV_p)^{m-k} \frac{m!}{(m-k)!k!} \tag{27}$$

The fraction of CWT is the probability of finding *no* randomly distributed LP in the scattering volume $P(0,n,V)$. For $m \gg 1$, which will normally hold because the LP values are normally much smaller than $V_s$, this is approximated, based on the above equation, as

$$P(0,m,n) \cong \exp(-nV_s) \quad m \gg 1 \tag{28}$$

In other words, the fraction of CWT decreases exponentially with the size of the scattering volume for a given $n$ and with increasing $n$ at fixed $V_s$.

Using exceptionally small $V_s$ could introduce uncertainties in the measurement of the BP scattering, due to particle number fluctuations within $V_s$. These are generally described by the Poisson distribution and are estimated as the square root of the number of particles in the scattering volume. In this work, however, even in the dilutest polymer solutions, the number fluctuation is negligible, since there are typically on the order of $10^9$ particles in $V_s$ (see below). This is expected generally to be the case when HTDSLS is used.

**Particle Counting for Flow Perpendicular to the Laser Beam.** In this work, a chamber was designed so that the particle flow was perpendicular to the scattering beam. The following considerations are hence made for this type of cell.

The key parameters which control LP detection are as follows: the scattering volume length, $z_m$; number density of LP, $n$; the speed of the LP, $v$; and the radius, $r(f)$, for which $f$ is a chosen value. The number of LP per second passing through a scattering volume defined by $f$ is

$$\dot{N}(f) = 2nvz_m r(f) \tag{29}$$

A particle passing through the center of the laser beam will give a spike of half-width

$$\Delta t_{1/2}(f) = \frac{w_o}{v}\sqrt{\frac{1}{2}\ln(1/f)} \tag{30}$$

This allows $v$ to be determined from a measurement of $\Delta t_{1/2}(f)$. It is noted that for capillary flow, where there is a uniform velocity distribution vs $r$, then $v = Q/A$, and it will not be necessary to know the beam waist to complete the analysis. In the current scattering chamber, this condition is not met, so that $v$ is determined via eq 30.

The limit of eq 30 for $f = 1$ deserves some comment, as $\Delta t_{1/2}(1) = 0$ by eq 30. Equation 30 applies for values of $f$, when the particle diameter $d_p$ is much smaller than $r(f)$ given by eq 22a, and the response time $\Delta t_r$, of the photodetector is much smaller than the $\Delta t_{1/2}$ of eq 30. In the limit as $f$ approaches 1, the measured value of $\Delta t_{1/2}$ will be equal to the convolution of the detector response function with the particle's scattering profile over a time interval of $d_p/v$. In this work we never need to work in the limit of such high values of $f$.

Now $r(f)$ can be expressed as

$$r(f) = w_o\sqrt{\frac{1}{2}\ln(1/f)} \tag{31}$$

so that

$$\dot{N}(f) = 2nvz_m w_o\sqrt{\frac{1}{2}\ln(1/f)} \tag{32}$$

The detection of LP in the scattering volume is predicated on the fact that a single particle passing through $V_s$ will give a scattering spike of maximum full-width duration $\Delta t_m$, if it passes through the center of the beam, and will be of less duration if it passes through the beam at a point not including the center. Notice that $\Delta t_m(f)$ is used to define $a(f)$, and is not meant to apply to the transit time of all particles within $a(f)$, which can be shorter. As discussed, single particle detection with simultaneous recovery of the background scattering level is assured only when there is an average of much less than one particle in the scattering volume, that is

$$nV_s \ll 1 \tag{33}$$

This is the criterion that dictates the range of LP concentrations that are measurable by the technique for an optically defined $V_s$ for a given instrument. As long as this condition holds, then each particle passing through the beam will produce an individual, resolvable spike (in fact, this condition does not have to be rigorously met, and eq 27 allows the probability to be assessed that a scattering spike is due to two or more particles simultaneously in the scattering volume). The frequency of spikes from intensities at and below $f$, $F(f)$, will be equal to $\dot{N}$ of eq 32 under this restriction.

Equation 32 allows the absolute concentration of scatterers to be determined when the particles are monodisperse. The proportionality constant $\gamma(f)$, between $F(f)$ and $n$ depends only on the known quantities $w_o$ and $z_m$, and on the readily measurable $v$

$$n = \frac{F(f)}{2vz_m w_o\sqrt{\frac{\ln(1/f)}{2}}} = \gamma(f)F(f), \quad nV_s \ll 1 \tag{34}$$

In the absence of knowledge of the value of n$V_s$, a restriction

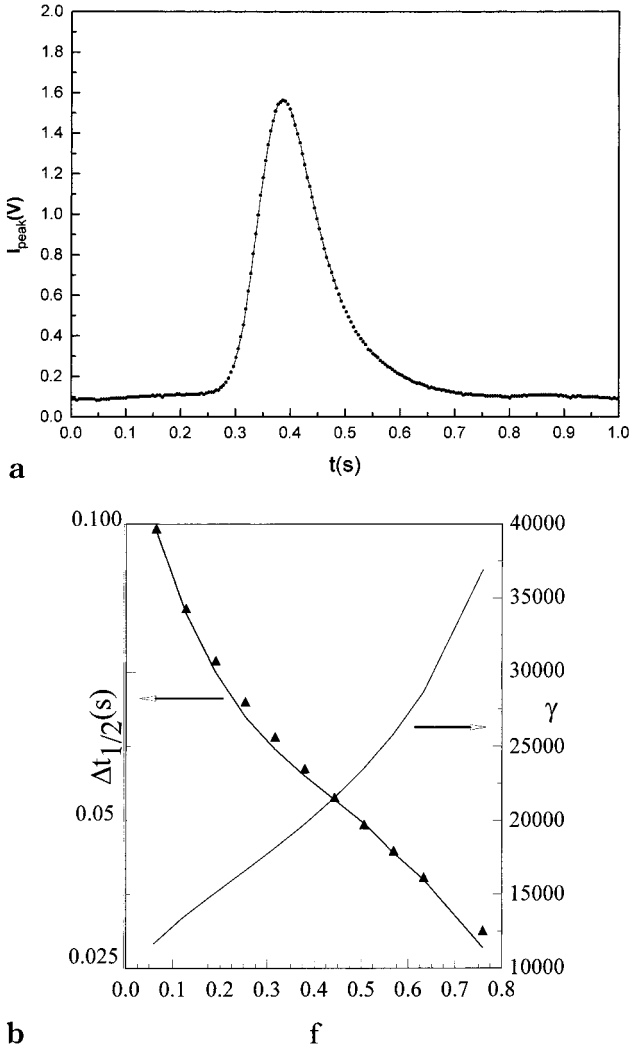


**Figure 1.** (a) Typical spike from a 2 $\mu$m latex sphere. Flow rate was 0.011 cm$^3$/s. Photodetector amplification was 100×. (b) The half-width $\Delta t_{1/2}(f)$ resulting from data such as in Figure 1a. The solid line with no symbols is the computation according to eq 30. The velocity resulting from this and the beam waist $w_o$ = 40 $\mu$m is $v$ = 0.048 cm/s ± 1.2%. Also shown is the conversion factor $\gamma(f)$ for this velocity.

can be put on the frequency itself, namely that

$$F \ll 1/\Delta t_m \quad \text{for single particle counting} \qquad (35)$$

When the inequality in eq 33 (or eq 35) no longer holds, $V_s$ will begin to saturate with LP and single particle counting will no longer be possible. The value of $V_s$ defined by eq 15 requires a criterion for determining the value of $r(f)$. The criterion is as follows. Having measured the peak scattering voltage of the LP, $V_s$ should be taken as the volume at whose defining radius $r(f)$, the remnant scattering intensity due to the LP, is less than the noise width of the scattering level due to the solvent and the BP. This will be illustrated with an experimental example in the Results and Discussion.

Figure 1a shows a typical scattering spike from a 2 $\mu$m latex sphere (the slight asymmetry is electronic in origin). Figure 1b shows the initial half-width $\Delta t_{1/2}(f)$ vs $f$, measured from Figure 1a, as well as a solid line computation using eq 30. Figure 1b also shows $\gamma(f)$, computed via eq 34.

Typical data for particle frequency $F(n,f)$ is shown for selected values of $f$ in Figure 2, where $n$ is the concentration of LP. As $n$ increases the scattering volume becomes saturated with particles. Saturation is reached when there is an average of one particle in the sampling volume during the transit time $\Delta t$. The saturation increases more rapidly the lower $f$ is, since

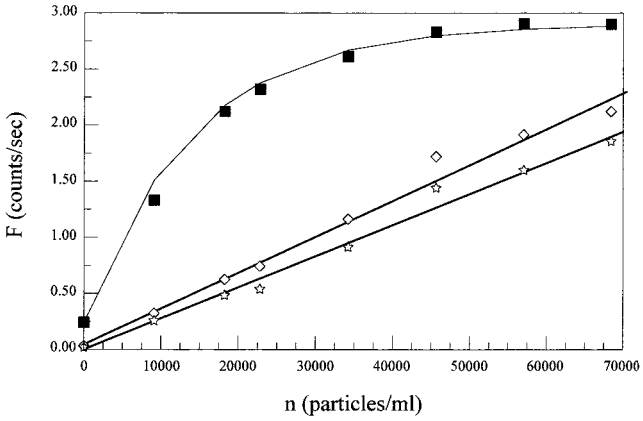


**Figure 2.** Particle count rate of 2 $\mu$m latex spheres vs relative particle concentration for three different peak cutoff values, from top to bottom; $f$ = 0.033, $f$ = 0.2, $f$ = 0.333. $Q$ = 0.011cm$^3$/s. The count rate increases linearly with particle concentration for the higher values of $f$, whereas the exponential approach to saturation is seen in the $f$ = 0.033 case. The peak voltage was 15.8 V.

lower $f$ corresponds to a larger scattering volume. Saturation occurs when the measured frequency equals $1/\Delta t_m$. The probability that there is one or more particles in the scattering volume is obtained from eq 28, and so

$$F_{max}\Delta t_m = 1 - e^{-nV_s} \qquad (36)$$

The upper curve in Figure 2 shows data where $n$ approaches the saturation limit. A two-parameter fit can be made for the maximum frequency $F_{max}$ and $V_s$. The linear portion of $F$ vs $n$ is achieved for the lower curves in Figure 2, where $f$ is sufficiently large.

**Spike Discrimination.** To count LP spikes, a spike discrimination and counting algorithm was implemented. The spike recognition algorithm established a baseline level and a cutoff level above the baseline in terms of fraction of maximum peak height $f$. Then, each point was examined sequentially. If a point was above the cutoff, the beginning of a peak was identified and the peak counter incremented by one. Successive points of positive slope did not alter the peak count, nor did points of decreasing slope. When the slope switches from negative back to positive (always for points above the cutoff) then the peak counter was incremented again.

To establish $F(f)$, each scattering spike at and above the threshold voltage corresponding to a chosen value of $f$ was assigned a frequency equal to the time interval between it and the previous spike. The data were then averaged in 200 s swaths.

A related issue is to find the peak height distribution arising from a particular laser beam intensity profile in the scattering volume as a population of uniform LP pass through it. Because a cutoff intensity level is sufficient to count peaks within a given scattering volume, the distribution is not necessary, and is not pursued here.

## Results and Discussion

**Equilibrium Characterization of a Heterogeneous Colloid and Polymer Solution.** To demonstrate the ability of the technique to make useful simultaneous measurements of particle density and absolute polymer characterization for a system in equilibrium, two experiments were performed: (1) a full Zimm plot determination of a polymer (PVP) coexisting with a colloid (2 $\mu$m latex spheres), and (2) fixed concentration of polymer with increasing amounts of added colloid.

Figure 3 shows the Zimm plot resulting from PVP solutions containing no latex spheres. The values are $M_w$ = 673 000 g/mol, $\langle S^2\rangle^{1/2}$ = 524 Å,and $A_2$ = 3.14 ×

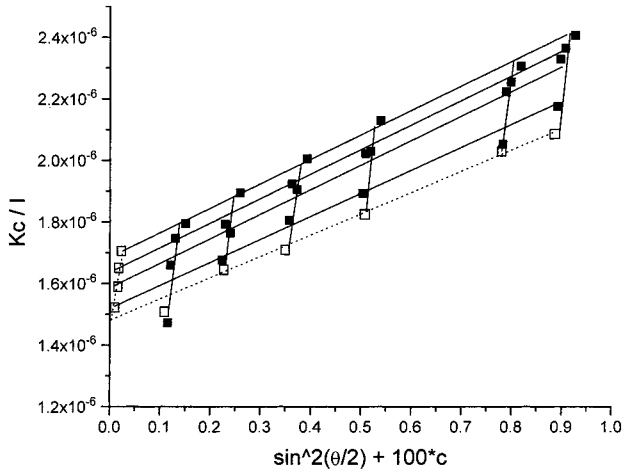


**Figure 3.** Zimm plot for pure PVP. $M_w = 673{,}000$, $\langle S^2\rangle^{1/2} = 524$ Å, and $A_2 = 3.14 \times 10^{-4}$. Concentrations are 0.04, 0.1, 0.2, and 0.4 mg/mL.

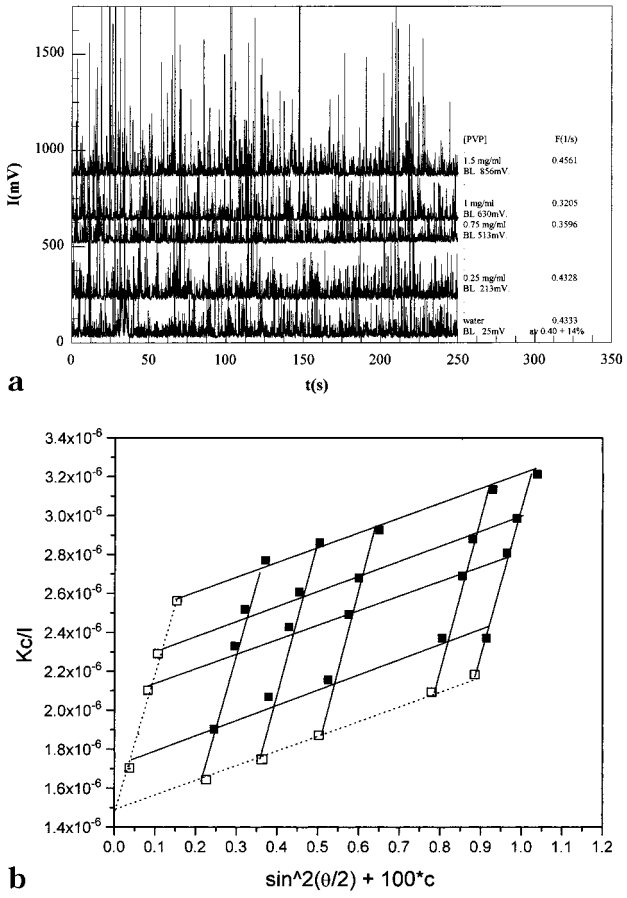


**Figure 4.** (a) Raw data for a mixture of PVP and 2 $\mu$m latex spheres at a concentration of 5120 particles/cm$^3$. $Q = 0.011$ cm$^3$/s. The average frequency was $F(0.1) = 0.40 \pm 14\%$, which corresponds to an absolute concentration (via $\gamma(f)$ from Figure 1b) of 5120. (b) Zimm plot resulting from the data in Figure 5a. Concentrations used are shown in Figure 4a. $M_w = 606\,000$ g/mol, $\langle S^2\rangle^{1/2} = 462$ Å, and $A_2 = 3.34 \times 10^{-4}$ cm$^3$ mol/g$^2$.

$10^{-4}$ cm$^3$ mol/g$^2$ and are in excellent agreement with extensive measurements recently made on the same material using an automated Zimm determination technique.[37]

Figure 4a shows data that result from a PVP solution containing 5120 latex spheres/cm$^3$. It is seen that there is sufficient CWT to determine the baseline scattering from the pure PVP. Figure 4b shows the Zimm plot

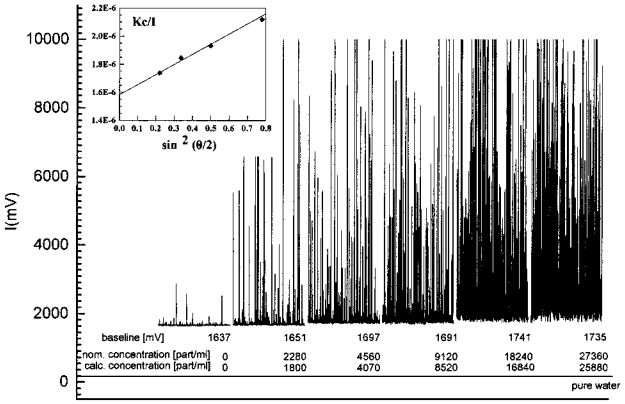


**Figure 5.** At a fixed concentration of PVP, the concentration of latex spheres is increased. from 0 to ~26 000 particles/cm$^3$. $Q = 0.0125$ cm$^3$/s. 100 s swaths of data are shown for the increasing sphere concentrations. Inset shows $Kc/I$ vs $q^2$, yielding $M_w = 661\,000$ g/mol, $R_g = 458$ Å, and $f = 0.1$ in determining the frequencies leading to the computed concentrations ($\gamma(0.1) = 11\,300$ at this $Q$).

resulting from these data. The values are $M_w = 606\,000$ g/mol, $\langle S^2\rangle_z^{1/2} = 462$ Å, and $A_2 = 3.34 \times 10^{-4}$ cm$^3$ mol/g$^2$, in reasonable agreement with those determined in Figure 3 in the absence of spheres.

It is useful to estimate the quantity $nV_s$ in the inequality in eq 33 and the scattering per particle of BP and LP. On the 100× photodetector amplification used for the data of Figure 4a, the maximum LP scattering signal was 1500 mV, and the net scattering level for solvent and 0.25 mg/mL PVP (BP) was 213 mV, with a standard deviation in the fluctuations of this value (in the absence of spheres) of approximately 5 mV. At the 5 mV level, $f = 0.00333$, so that by eq 31, $r(0.00333) = 1.69w_o$ or $r(0.00333) = 68$ $\mu$m, using $w_o = 40$ $\mu$m. At this value of $r$, $V_s = 2.76 \times 10^{-5}$ cm$^3$, using the scattering volume length of 0.19 cm, so that the inequality in eq 33 demands that $n \ll 1/V_s = 36\,000$ particles/cm$^3$, which is reasonably well fulfilled for the concentration of 5120 LP particles/cm$^3$ used. At this concentration eq 28 indicates that the fraction of CWT is 0.86.

To estimate the ratio of scattering from a single polymer to a single LP, it is necessary to know the average scattering intensity over the scattering volume $V_s$. It is straightforward to show that the volume averaged intensity $\langle I\rangle_{Vol}$ for the intensity profile given by eq 14 over a cylindrical scattering volume (i.e., $w(z) = w_o$ in eq 14) of radius $r = \xi w_o$ is

$$\langle I\rangle_{Vol} = \frac{I_o}{2\xi^2}[1 - e^{-2\xi^2}] \qquad (37)$$

Hence, a single sphere, with a maximum scattering voltage of 1.500 V gives an average scattering signal of $V = 0.260$ V per LP for $\xi = 1.69$, whereas the PVP in the same volume gives 0.213 V. There are about $6.85 \times 10^9$ PVP chains in the $V_s$ corresponding to $\xi = 1.69$, which yields $3.11 \times 10^{-11}$ V/PVP polymer chain (ignoring the $A_2$ correction), giving $8.4 \times 10^9$ times more scattering for a 2 $\mu$m latex sphere than a single PVP chain.

Figure 5 shows raw data for PVP at 0.1 mg/cm$^3$ with increasing amounts of added 2 $\mu$m latex spheres, from 0 to ~26 000 particles/cm$^3$. The approach to the saturation of the scattering volume is seen at concentrations of 16 800 particles/cm$^3$, where CWT diminishes, and is

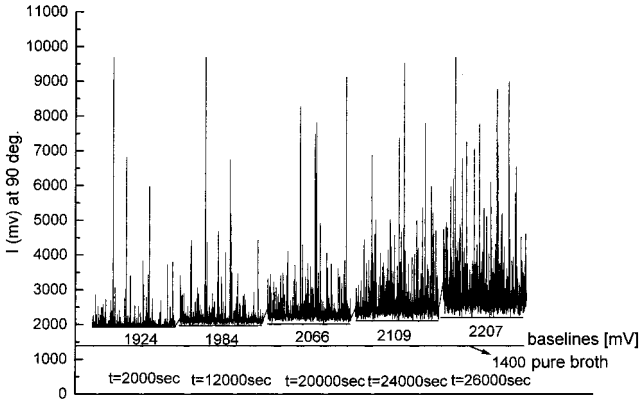


**Figure 6.** 100 s swaths of data, at the times indicated, from raw spike spectrum at $\theta = 90°$ for growing *E. coli* with 0.1 mg/mL PVP at $T = 38$ °C, $Q = 0.0125$ cm$^3$/s, and starting *E. coli* concentration of 840 per cm$^3$ (0.02 cts/s, $\gamma = 41\,800$).

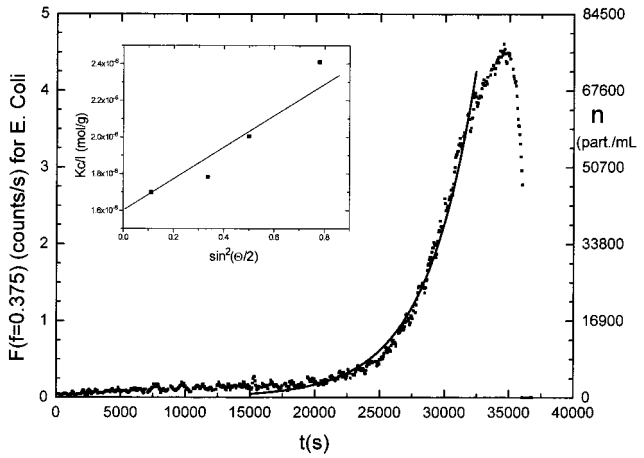


**Figure 7.** Growth curve for data from Figure 7, at $\theta = 90°$ for cutoff level 1.5 V corresponding to $f = 0.375$. $Q = 0.0125$ cm$^3$/s, and $\gamma(f) = 16\,900$. Left axis shows $F(0.375)$; right axis is the absolute bacteria concentration. The doubling time is 45 min. The inset shows the PVP scattering recovered from the CWT in Figure 7. It gives $M_w = 644\,000$ g/mol and $R_g = 437$ Å.

finally lost at the highest concentration. The inset shows $Kc/I$ vs $q^2$ for these data, and, using the value of $A_2$ of $3.34 \times 10^{-4}$ cm$^3$ mol/g$^2$, allows the following values to be obtained, $M_w = 661\,000$ g/mol and $R_g = 458$ Å, which are also in good agreement with the values determined in the absence of spheres.

The ability of the system to discriminate colloids and polymers is useful not only for the cases where the colloids represent an interesting population in themselves but also for making equilibrium measurements on polymers even when high levels of particulate contamination exist.

**Heterogeneous Time Dependent Light Scattering on a Biological Test System.** To demonstrate the time dependent capabilities of the system, a growing *E. coli* population was mixed with a fixed 0.1 mg/mL concentration of PVP. Control tests with and without PVP showed that the *E. coli* growth rate is not measurably affected by PVP.

Figure 6 shows 100 second wide swaths of raw data at different times for growing *E. coli* at $T = 38$ °C for the $\theta = 90°$ detector. The sampling rate was every 0.055 s and the flow rate was 0.0125 cm$^3$/s.

Figure 7 shows the count rate $F$ vs time for these data, using the $f = 0.375$ level (1.5 V above baseline), and

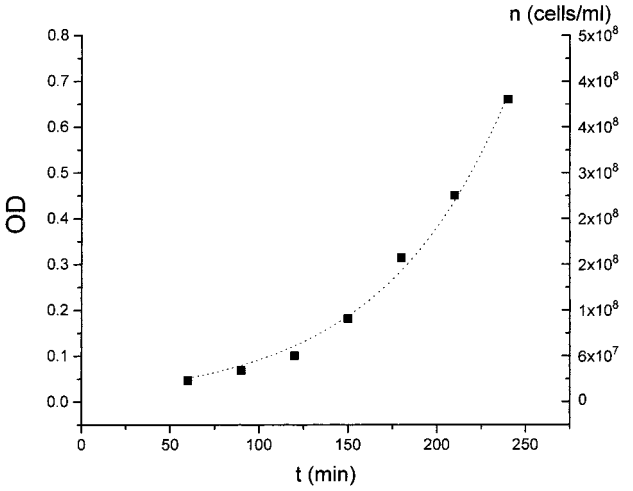


**Figure 8.** Spectrophotometer growth curve for *E. coli* at $T = 37$ °C. Optical density, OD, was at 600 nm. Doubling time = 45.6 min. The right-hand axis shows the approximate bacterial concentration.

subtracting off the 0.05 counts/s background scattering. This background scattering is due to dust and other impurities in the medium, which are not removed because no on-line filter was used. Also shown is the absolute particle concentration using $\gamma = 16\,900$, appropriate for this cutoff level on this detector at the stated flow rate. There is apparently an incubation period before the cells begin to propagate. The characteristic, exponential doubling time, once the exponential growth region begins, was 45 min. The averaging period of 200 s was much smaller than this growth period. Toward later times the saturation of the scattering volume is apparent. At full saturation there are no peaks to distinguish, and $F$ plunges to zero.

The inset of Figure 7 shows the scattering recovered from the PVP. Using a linear fit gives $M_w = 644\,000$ and $R_g = 437$ Å, which are in good agreement with the values of PVP measured with no LP present. It is also interesting to note that even as saturation of the scattering volume is approached in Figure 6 the baseline needed for recovery of the BP only increases by about 14%. Some of the increase may be due to polymeric or other products excreted by the bacteria, although the increase is most likely due to the contribution to the baseline from the remnant scattering of many particles in the outer fringes of the laser beam, since the product $nV_s$ becomes signficantly greater than unity in the later stages of the *E. coli* growth. Estimates of the increase in background due to saturation effects could be made via eqs 14 and 27, but are not pursued here. An encouraging result is that even though exact baseline determination becomes compromised as the inequality in eq 33 is exceeded when using the $V_s$ determined by the baseline fluctuation criterion discussed earlier, effective particle counting can nonetheless occur well beyond that limit, since choosing higher values of $f$ reduces the value of $V_s$ within which particle counting is done.

Data taken at different angles (not shown) yielded the same type of growth curves with similar exponential growth constants. Since the scattering volume is larger away from $\theta = 90°$, the scattering volume saturates with *E. coli* at lower concentrations than at $\theta = 90°$, for a given value of $f$.

Finally, Figure 8 shows a spectrophotometric deter-

mination of the *E. coli* growth rate. The doubling time is the same as determined by HTDSLS. The optical density was measured at 600 nm. Roughly, 1 O. D. at this wavelength corresponds to $8 \times 10^8$ cells/cm$^3$ (ref 36, p 61). The approximate particle concentration is shown on the right-hand side of the axis. There is a striking difference of nearly 4 orders of magnitude between the low particle densities that can be determined by HTDSLS and the high densities needed for optical density measurements. HTDSLS also gives the characterization of the coexisting polymer, to which optical density measurements are insensitive.

## Summary

The feasibility of simultaneously determining the number density of colloid particles and the molecular characteristics of a coexisting polymer population has been demonstrated. Relative motion between particles and the incident laser beam to produce scattering spikes from the colloid has been provided by flow in this case. In principle, any scheme for relative motion will work, and moving the laser/detector might be preferable in some instances, e.g., where shear sensitivity of the sample is of concern or the sample is otherwise "anchored".

This ability of the HTDSLS technique was first used to determine the properties of a polymer population, even in the presence of significant particulate contaminants. This feature alone, should allow the use of traditional SLS in systems previously considered too "dusty" for proper measurement. The second demonstration of HTDSLS was to measure the growth rate of a bacterial population (*E. coli*), while continuously recovering the properties of a coexisting polymer population.

This first demonstration of the technique was restricted to determining the density of large particles and the absolute characteristics of the coexisting polymer population. It is left to near-term future work to develop the optical characteristics of the chamber so that quantitative Mie characterization can also be carried out on the LP.

**Acknowledgment.** Support from the Louisiana Board of Regents University/Industrial Ties (RD-B-11) and the National Science Foundation (9877206) is gratefully acknowledged. R. Schimanowski acknowledges the Evangelisches Studienwerk (Germany) for partial support. We thank Professor Mark Millonas for help with spectrophotometric assays of *E. coli* growth.

## References and Notes

(1) Florenzano, F. H.; Strelitzki, R.; Reed, W. F. *Macromolecules* **1998**, *31*, 7226−7238.
(2) Reed, C. E.; Reed, W. F. *J. Chem. Phys.* **1989**, *91*, 7193−7199.
(3) Reed, W. F. *J. Chem. Phys* **1995**, *103*, 7576−7584.
(4) Catalani, L. H.; Rabello, A. M.; Florenzano, F. H.; Politi, M. J.; Reed, W. F. *Int. J. Polym. Charact. Anal.* **1997**, *3*, 231−247
(5) Ghosh, S.; Reed, W. F. *Biopolymers* **1995**, *35*, 435−450.
(6) Holthoff, H.; Egelhaaf, S. U.; Borkovec, M.; Schurtenberger, P.; Sticher, H. *Langmuir* **1996**, *12*, 5541−5549
(7) Wright, L. S.; Chowdhury, A.; Russo, P. *Rev. Sci. Instrum.* **1996**, *67*, 3645−3648.
(8) Egelhaal, S. U.; Schurtenberger, P. *Rev. Sci. Instrum.*, **1996**, *67*, 540−545.
(9) Norisuye, T.; Shibayama, M.; Nomura, S. *Polymer* **1998**, *39*, 13, 2769−2775.
(10) Vinches, C.; Parker, A.; Reed, W. F. *Biopolymers* **1997**, *41*, 607−622.
(11) Dautzenberg, H.; Rother, G. *J. Appl. Polym. Sci.; Appl. Polym. Symp.* **1991**, *48*, 351−369
(12) Zimm, B. H. *J. Chem. Phys.* **1948**, *16*, 1093−1115.
(13) Kerker, M. *The Scattering of Light and Other Electromagnetic Radiation*; Academic Press: New York, 1963.
(14) Van de Hulst, H. C. *Light Scattering by Small Particles*; John Wiley and Sons: New York, 1957.
(15) Moldovan, A. *Science* **1934**, *80*, 188−189.
(16) Lines, R. *Process Eng.* **1990**, *71*, 56−74.
(17) Nicoli, D. F.; Kourti, T.; Gossen, P.; Wu, J.-S.; Chang, Y.-J.; MacGregor, J. F. *On-Line Particle Size Distribution by Dynamic Light Scattering*; ACS Symposium Series 472; Provder, T., Ed.; American Chemical Society: Washington, DC, 1991; pp 86−97.
(18) Coulter, W. H. *Proc. Nat. Electron. Conf.* **1956**, *12*, 1034.
(19) Kubitschek, H. E. *Nature* **1958**, *182*, 234−235.
(20) Gear, A. R. L.; Bednarek, J. M. *J. Cell. Biol.* **1972**, *54*, 325−345.
(21) Bryant, F. D.; Seiber, B. A.; Latimer, P. *Arch. Biochem. Biophys.* **1969**, *135*, 97−108.
(22) Rochon, P.; Racey, T. J.; Zellar, M. *Appl. Opt.* **1988**, *27*, 3295−3298.
(23) Kaye, P. H. *Meas. Sci. Technol.* **1998**, *9*, 141−149.
(24) Gebhart, J.; Bol, J.; Heinze, W.; Letschert, W. *Staub-Reinhalt. Luft* **1970**, *30*, 5−14.
(25) Sommer, H. T.; Harrison, C. F.; Montague, C. E. *Spec. Publ.—R. Soc. Chem.* **1992**, *102*, 163−172
(26) Wyatt, P. J. *J. Colloid. Interface Sci.* **1972**, *39*, 125−135.
(27) Diehl, S. R.; Smith, D. T.; Sydor, M. *Appl. Opt.* **1979**, *18*, 1653−1658.
(28) Marshall, T. R.; Parmenter, C. S.; Seaver, M. *J. Colloid. Interface Sci.* **1976**, *55*, 624−636.
(29) Wyatt, P. J.; Scherer, K. L.; Phillips, S. D.; Jackson, C.; Chang, Y.-J.; Parker, R. G.; Phillips, R. G.; Bottiger, J. R. *Appl. Opt.* **1988**, *27*, 217−221.
(30) Hirst, E.; Kaye, P. H. *J. Geophys. Res. (Atmos.)* **1996**, *101 D 19*, 231−235.
(31) Holve, D.; Self, S. A. *Appl. Opt.* **1979**, *18*, 1632−1652.
(32) Bader, H.; Gordon, H. R.; Brown, O. B. *Rev. Sci. Instrum.* **1972**, *43*, 1407−1412.
(33) Steinkamp, J. A. *Rev. Sci. Instrum.* **1984**, *55*, 1375−1400.
(34) Seo, J.-H.; Bailey, J. E. *Biotech. Bioeng.* **1987**, *30*, 297−305.
(35) Cross, D. A.; Latimer, P. *Appl. Opt.* **1972**, *11*, 1225−1228.
(36) Maniatis, T.; Fritsch, E. F.; Sambrook, J. *Molecular Cloning*; Cold Spring Harbor Laboratory: Cold Spring Harbor, NY, 1982.
(37) Strelitzki, R.; Reed, W. F. *J. Appl. Polym. Sci.* **1999**, *73*, 2359−2368.

MA9907690